Published in final edited form as:

Chem Mater. 2018 ; 30(18): . doi:10.1021/acs.chemmater.8b03283.

Opposite Thermal Expansion in Isostructural Noncollinear Antiferromagnetic Compounds of Mn_3A (A = Ge and Sn)

Yuzhu Song[†,‡], **Yongqiang Qiao**[‡], **Qingzhen Huang**[§], **Chinwei Wang**[‖], **Xinzhi Liu**[⊥], **Qiang Li**[‡], **Jun Chen**[*,†,‡], **Xianran Xing**[†,‡]

[†]Beijing Advanced Innovation Center for Materials Genome Engineering, University of Science and Technology Beijing, Beijing 100083, China

[‡]Department of Physical Chemistry, University of Science and Technology Beijing, Beijing 100083, China

[§]NIST Center for Neutron Research, National Institute of Standards and Technology, Gaithersburg, Maryland 20899-6102, United States

[‖]Neutron Group, National Synchrotron Radiation Research Center, Hsinchu 30077, Taiwan

[⊥]Helmholtz-Zentrum-Berlin für Materialien und Energie, Hahn-Meitner-Platz 1, D-14109 Berlin, Germany

By virtue of the inherent anharmonic lattice dynamics, the volume of most solids expands upon heating. It is unconventional to find solids with negative thermal expansion (NTE), i.e., solids in which the distances between atoms decrease with increasing temperature.[1–3] NTE materials have crucial technological applications in the control of thermal expansion. In 1996, isotropic NTE was discovered in ZrW_2O_8.[1] In the past two decades, NTE has been found in various types of materials, such as oxides,[4–7] alloys,[8–13] nitrides,[14,15] fluorides,[16–18] and cyanides.[19–22] In essence, the thermal expansion of a solid is affected by a complex interplay between the electrons, phonons, and lattice.[2] The NTE phenomenon originates from diverse factors such as an open-framework,[17,19] the size effect,[23] charge transfer,[5,6] magnetism,[12–14,24] ferroelectricity,[7] and superconductivity.[25,26] Obviously, most of the NTE solids are inorganics, which have relatively strong chemical bonds.

It is known that solids with weak bonds exhibit a strong positive thermal expansion (PTE).[27] For example, due to their weak metallic bonds, metals based compounds generally have a strong PTE, e.g., Al $\left(\alpha_l = 23.1 \times 10^{-6}/\mathrm{K}\right)$, Cu $(\alpha_l = 17.7 \times 10^{-6}/\mathrm{K})$, and Fe $(\alpha_l = 11.8 \times 10^{-6}/\mathrm{K})$.[28] To meet the requirement for a low coefficient of thermal expansion (CTE), metal matrix composites (MMCs) are often fabricated by adding fillers with low or negative thermal expansion,[29] such as Cu/ZrW_2O_8 composites,[30] Al(Si)/Diamond,[31] Al/

[*]Corresponding Author: J. Chen. junchen@ustb.edu.cn.

ASSOCIATED CONTENT

Supporting Information

The Supporting Information is available free of charge on the ACS Publications website at DOI: 10.1021/acs.chemmater.8b03283.

Materials synthesis, experimental methods, data analysis procedures (PDF)

The authors declare no competing financial interest.

stainless-invar,[32] and Al/SiC.[33] It is well-known that metals based compounds are normally benefitted by advantages such as high mechanical strength and good electrical and thermal conductivities. Therefore, it is imperative that NTE metals based compounds be found. For example, the Invar alloy $Fe_{0.65}Ni_{0.35}$, which was found in 1897, has been a popular topic of fundamental studies and practical applications over the last century. Because of this discovery, Swiss scientist C. É. Guillaume won a Nobel Prize in Physics in 1920.[34] However, rare NTE metals based compounds have been found, such as Invar alloys,[8] R_2Fe_{17} (R = rare earth elements),[9] (Hf,Nb)Fe_2,[10] MnCoGe-based compounds,[11] La(Fe,Si,Co)$_{13}$,[12] and Tb-(Co,Fe)$_2$.[13] Note that all of these NTE metals based compounds are ferromagnetic.

Here, we report an intriguing NTE in the noncollinear antiferromagnetic intermetallic compounds of Mn_3Ge. For a better understanding on the NTE mechanism of Mn_3Ge, the isostructural compound of Mn_3Sn showing PTE has also been studied for comparison. Their complicated triangular antiferromagnetic (AFM) structure and NTE mechanism are revealed via a combined analysis of the temperature dependence of neutron powder diffraction (NPD), synchrotron X-ray diffraction (SXRD) and macroscopic magnetic measurements. The direct link between the NTE behavior and the magnetic structure, which is correlated to the magnetovolume effect (MVE), is demonstrated. Particularly, the present NTE Mn_3Ge exhibits excellent mechanical properties and good thermal and electron conductivity behaviors.

A series of single-phase $Mn_3(Ge_{1-x}Sn_x)$ ($x = 0.0,\ 0.2,\ 0.4,\ 0.6,\ 0.8,$ and 1.0) samples were prepared via arc melting. The crystal structure was identified via high-intensity SXRD (Figure S1a). To determine the precise magnetic and crystal structure of both Mn_3Ge and Mn_3Sn, the temperature dependence of NPD has been carried. Mn_3Ge remains in a single phase with a hexagonal structure (space group: $P6_3/mmc$) over the whole temperature range. Mn and Ge atoms occupy Wyckoff sites 6h ($x,\ 2x,\ 1/4$) and 2c($1/3,\ 2/3,\ 1/4$), respectively (inset of Figure 1). By comparing the NPD patterns at typical low and high temperatures (150 and 500 K, respectively), the magnetic structure makes only an additional intensity contribution to the nuclear peaks, and no additional peaks can be observed. Therefore, the propagation vector of the Mn_3Ge magnetic structure is $k = (0,\ 0,\ 0)$ (Figure S2). Its crystal structure consists of alternating layers of manganese triangles, stacked parallel to the c axis. Because of the geometrical frustration, three neighboring spins cannot be pairwise antialigned on a triangular lattice.[35] Therefore, only the triangular antiferromagnetic structures are compatible. Some of the possible magnetic structural models allowed by the symmetry of the $P6_3/mmc$ structure and its subgroups are listed in Figure S3. Among these AFM spin configurations, the structural model of Figure S 3f gives the best refinement. Figure 1 presents the magnetic structure refinements of the NPD pattern for Mn_3Ge. The Mn moments of inverse triangular antiferromagnetic order are along the [110] direction, and the spins rotate 120° counterclockwise in the ab plane (the inset of Figure 1). It needs to note that the magnetic structure of Mn_3Ge is similar to the previous studies.[36,37]

Intriguingly, Mn_3Ge exhibit a strong NTE property. No structure phase transition occurs in the NTE temperature range. The average linear CTE of Mn_3Ge is $\alpha_l = -7.58 \times 10^{-6} K^{-1}$ ($297 - 374$ K), which was determined via a macroscopic thermo-dilatometer measurement

(Figure 2). However, the isostructural compound of Mn_3Sn shows an opposite PTE at the whole temperature range. Two inflection points are associated with the magnetic transitions. The temperature dependence of the unit cell volume, which was determined via NPD, can also confirm the reliability of NTE (Figure 4b). As a comparison, the present Mn_3Ge exhibits an NTE magnitude similar to that of other typical NTE inorganics, such as ScF_3 ($\alpha_l = -7.47 \times 10^{-6}K^{-1}$, 150 – 425 K)[16,38] and ZrW_2O_8 ($\alpha_l = -9.1 \times 10^{-6}K^{-1}$, 10 – 300 K).[1] Note that most available NTE alloys are ferromagnetic (FM), whereas the present Mn_3Ge exhibits an antiferromagnetic structure. Furthermore, even a high Neel temperature (T_N) is found in the present Mn_3Ge (T_N = 380 K) when compared with other antiferromagnetic intermetallic compounds, such as YMn_2 (T_N = 100 K),[39] Gd_5Ge_4 (T_N = 125 K),[40] and $CeFe_2$ ($T_N \sim 90$ K).[41] Because of the magnetostriction effect, the dimensions of FM alloys can be influenced by the external magnetic field. However, AFM compounds can avoid the negative effect of the external magnetic field on the precise dimension.

The macroscopic magnetic behavior of Mn_3Ge was studied by measuring the temperature dependence of magnetization (zero-field-cooling (ZFC) and field-cooling (FC) modes) (Figure S5a). An obvious peak of the ZFC curve (100 Oe) can be seen, which reveals the feature of the AFM transition. The Neel temperature T_N is determined to be 370 K. With increasing external magnetic field, the magnetization of the residual FM component is increased, which overwhelms the signal of the AFM structure. Note that the very small residual FM component is caused by a small distortion of the hexagonal structure.[42] Furthermore, the magnetic transition temperature is hardly changed by the external magnetic field, which verifies the stability of the triangular antiferromagnetic structure. Isothermal magnetization curves of Mn_3Ge measured at various temperatures are shown in Figure S6. The dominating AFM nature is clearly indicated by the linear and unsaturated magnetization behavior at higher fields. In Figure S5b, there are two obvious magnetic transitions at 255 K and above 400 K for Mn_3Sn, which are consistent with the dilatometer result. In addition, the magnetic transition temperature of Mn_3Ge is close to the disappearing temperatures of NTE (Figure 2 and Figure S5), indicating that the anomalous thermal expansion phenomenon of Mn_3A (A = Ge, Sn) is entangled with the magnetic behavior.

In the purpose of explaining opposite thermal expansion in the isostructural noncollinear antiferromagnetic intermetallics of Mn_3A (A = Ge and Sn), the microscopic thermal expansion information was extracted from the results of magnetic structure refinement of high-intensity NPD (Figure S4). The temperature dependence of the lattice parameters extracted from the NPD data is shown in Figure S7. Obviously, the NTE of Mn_3Ge is dominated by the shrinking of the *a*(*b*) axis; nevertheless, the *c* axis linearly expands. However, in Mn_3Sn both *a*(*b*) and *c* axes linearly expand. It means that such opposite thermal expansion is correlated to the *ab* plane.

To study the detailed behavior for the shrinkage of the *ab* plane, the bond distances between different magnetic atoms (Mn) were extracted from variable temperature NPD data. Figure 3a shows a $4 \times 4 \times 1$ supercell of the *ab* plane for Mn_3A (A = Ge and Sn), d_1 and d_2 sign the bond distances of Mn–Mn (I) and Mn–Mn (II), respectively. As shown in Figure 3b,c, d_1 always increases in the whole temperature range for both Mn_3Ge and Mn_3Sn.

However, d_2 takes place to shrink at different level below magnetic transition temperature. The total change of d_1 and $d_2(\Delta d_1 + \Delta d_2)$ shows the same behavior with that of the *a* axis, which exhibits NTE for Mn_3Ge but PTE for Mn_3Sn below magnetic transition temperatures (Figure 3d). Therefore, the NTE of Mn_3Ge is due to the decrease in the bond distance d_2, which is caused by MVE.

The more detailed magnetic and crystal structure information was extracted from NPD data to reveal the detailed MVE of Mn_3Ge and Mn_3Sn. As shown in Figure 4a, it is interesting to note that the Mn moments of Mn_3Ge and Mn_3Sn are nearly identical at 275 K, but nonlinearly decrease and vanish at $T_N = 380$ K for Mn_3Ge and $T_N = 420$ K for Mn_3Sn. It seems that the AFM order can be more easily disturbed in Mn_3Ge than Mn_3Sn. Figure 4c shows the strong coupling role between magnetism and lattice in the NTE Mn_3Ge. As the Mn magnetic moment drops slowly at low temperatures (below 275 K), the lattice parameter *a* expands, i.e., PTE occurs; however, when the magnetic moment drops quickly (275–375 K), *a* begins to shrinks, i.e., NTE happens. To further study the relation between magnetism and thermal expansion, the trends of dM/dT and $d(\Delta l/l)/dT$ are calculated for both Mn_3Ge and Mn_3Sn (Figure 4d). Clearly, a similar tendency can be observed in both magnetic moment and macroscopical thermal expansion of Mn_3A (A = Ge and Sn) as a function of temperature. With increasing temperature, the magnetic moment decreases rapidly or slowly, the property of thermal expansion changes accordingly. The rate of magnetic transition dominates the thermal expansion of Mn_3A (A = Ge and Sn), which is directly associated with the Mn moments lying the *ab* plane. The rate of magnetic transition (dM/dT) in NTE Mn_3Ge is stronger than that of PTE Mn_3Sn, which means a stronger contribution of spontaneous magnetostriction to thermal contraction. Therefore, the bonds of Mn–Mn (d_2) in Mn_3Ge shrink more obviously than Mn_3Sn, which exceeds the expansion of the bond distance d_1. The NTE occurs in Mn_3Ge (Figure 3).

In other words, the Wigner–Seitz volume of Mn_3Sn is expanded due to the existence of bigger Sn atoms, resulting in the increase of Mn–Mn bond length (Figure S1). The longer of Mn–Mn distance makes the antiferromagnetic exchange interaction stronger in Mn_3Sn, which is also evidenced by the higher $T_N = 420$ K in Mn_3Sn compared with $T_N = 380$ K in Mn_3Ge. Theoretically, when the exchange interaction is enhanced, the compound needs more energy to break magnetic ordering. Therefore, the spins of Mn_3Sn depart from parallel alignment more difficultly than Mn_3Ge with increasing temperature, i.e., the rate of magnetic transition (dM/dT) in Mn_3Sn is slower than that of Mn_3Ge (Figure 4d). It is known that magnetic configuration with aligned spins has a larger volume than that with disordered spins,[24] which means the magnetic transition brings a negative contribution to thermal expansion. Because of the faster magnetic transition, the contribution to lattice change from magnetic order overwhelms that from lattice thermal vibration. As a result, the overall thermal expansion of Mn_3Ge becomes negative (Figure 4b). However, the spontaneous magnetostriction of Mn_3Sn is relatively weak, which cannot overcome positive contribution to thermal expansion from lattice vibration. PTE happens at the whole temperature range. The change of magnetic moment control the NTE property should be the common feature for most magnetic NTE compounds, such as Mn_3AN.[43–45]

To quantify the relationship between magnetic contribution and thermal expansion, spontaneous magnetostriction (ω_s) is used to quantitatively describe the contribution of MVE to anomalous thermal expansion.[46,47] The value of ω_s is calculated by $\omega_s = \omega_{exp} - \omega_{nm}$, in which ω_{exp} is the experimental linear thermal expansion measured by thermos-dilatometer, and ω_{nm} is the linear thermal expansion of a nonmagnetic reference.[48] As shown in Figure S8, the NTE property of Mn_3Ge can be regarded as a combined result of ω_s and lattice vibration (ω_{nm}). Here, temperature dependence of both the square of Mn moment $\left(M^2\right)$ and ω_s is performed for the detailed analysis of NTE mechanism of Mn_3Ge. As depicted in Figure 5a,b, it is obvious to reveal a strong linear correlation between M^2 and ω_s, which can be quantitatively ascribed by the equation of

$$\omega_s(T) = kCM(T)^2 \quad (1)$$

where k and C are the compressibility and the magnetovolume coupling constant, and $M(T)$ is the amplitudes of Mn magnetic moment.[49,50] It means that the magnetic contribution and the thermal expansion have a quantitative relationship, and thus thermal expansion can be tuned by changing the magnetic ordering.

From the practical application viewpoint, better performances in terms of high mechanical strength and good thermal and electron conductivity properties are demanded for NTE materials. The engineering stress–strain curves of Mn_3Ge ingots are shown in Figure S9. The maximum compressive strength can be as large as 204 MPa, together with a total elongation of 5.4%. As a comparison, the compressive strength of the Nd–Fe–B-based permanent magnets and that of the $La(Fe,Si)_{13}$-based magnetic refrigeration materials are 112 MPa, and 120 MPa, respectively.[51,52] It is well-known that intermetallic compounds are generally very fragile, and are thus unsuitable for compressive or tensile tests. In general, to improve the mechanical property of NTE intermetallic compounds, binder is often introduced to bond powders of alloys. For example, the as-prepared MnCoGe-based alloys are brittle and spontaneously fragment into powders. Their compressive strength increases to 70.4 MPa after using epoxy-binder as a bonder.[11] The temperature dependence of the metallic property of Mn_3Ge is also depicted in Figure S10. At room temperature, the thermal conductivity is $6.8\ W \cdot (m \cdot K)^{-1}$, which is much larger than that of most NTE inorganic compounds, such as the prototype NTE oxide of ZrW_2O_8 $\left(0.5\ W \cdot (m \cdot K)^{-1}\right)$ Furthermore, the electrical conductivity of the present NTE Mn_3Ge is $1 - 2 \times 10^3 (\Omega \cdot cm)^{-1}$. As a comparison, most NTE inorganic solids are insulating. Their electrical conductivity is linearly reduced upon heating, which reveals the characteristic of metallic conductivity.

The present Mn_3Ge exhibit a new and simple structure type for the NTE property, which yields a new class of antiferromagnetic NTE compounds. The control of thermal expansion can be achieved in Mn_3Ge-based compounds via chemical modification similar to that often utilized for NTE materials, such as ScF_3[16,17,38] and antiperovskites.[3,14,15] For example, the

solid solutions of $Mn_3(Ge_{1-x}Sn_x)$ have been investigated (Figure S1). Thermal expansion of $Mn_3(Ge_{1-x}Sn_x)$ gradually transforms from NTE to PTE with increasing Sn concentration.

In summary, a new and simple NTE structure type has been found in antiferromagnetic compounds of Mn_3Ge. The unusual inverse triangular antiferromagnetic structure of Mn_3Ge was confirmed via variable temperature NPD and macroscopic magnetic measurements. The direct experimental evidence reveals the contribution of the magnetovolume effect to the anomalous thermal expansion of Mn_3Ge, compared with the isostructural PTE Mn_3Sn. The NTE property of Mn_3Ge originates from the quick decrease of Mn moments which causes the shrink of the bond distances of Mn–Mn (d_2). The present NTE Mn_3Ge exhibits the antiferromagnetic property which can thus avoid the influence of the external magnetic field on the dimensions. Furthermore, the high mechanical properties and good metallic property of the present NTE Mn_3Ge provide a greater possibility for better industrial applications in the future.

Supplementary Material

Refer to Web version on PubMed Central for supplementary material.

ACKNOWLEDGMENTS

This work was supported by the National Natural Science Foundation of China (grant nos. 21731001 and 21590793), the Changjiang Young Scholars Award, and the Fundamental Research Funds for the Central Universities, China (FRF-TP-17-001B). This research used resources of the Advanced Photon Source, a U.S. Department of Energy (DOE) Office of Science User Facility operated for the DOE Office of Science by Argonne National Laboratory under Contract No. DE-AC02-06CH11357. The NPD data was collected at the high-intensity diffractometer Wombat of the Australian Nuclear Science and Technology Organisation (ANSTO) and the BT-1 neutron powder diffractometer at the NIST Center for Neutron Research.

REFERENCES

(1). Mary TA; Evans JSO; Vogt T; Sleight AW Negative Thermal Expansion from 0.3 to 1050 K in ZrW2O8. Science 1996, 272, 90–92.

(2). Chen J; Hu L; Deng J; Xing XR Negative Thermal Expansion in Functional Materials: Controllable Thermal Expansion by Chemical Modifications. Chem. Soc. Rev 2015, 44, 3522–3567. [PubMed: 25864730]

(3). Takenaka K Negative Thermal Expansion Materials: Technological Key for Control of Thermal Expansion. Sci. Technol. Adv. Mater 2012, 13, 013001. [PubMed: 27877465]

(4). Evans JSO; Hanson PA; Ibberson RM; Duan N; Kameswari U; Sleight AW Low-Temperature Oxygen Migration and Negative Thermal Expansion in ZrW2−xMoxO8. J. Am. Chem. Soc 2000, 122, 8694–8699.

(5). Long YW; Hayashi N; Saito T; Azuma M; Muranaka S; Shimakawa Y Temperature-Induced A–B Intersite Charge Transfer in an A-Site-Ordered Lacu3fe4o12 Perovskite. Nature 2009, 458, 60–63. [PubMed: 19262669]

(6). Azuma M; Chen WT; Seki H; Czapski M; Olga S; Oka K; Mizumaki M; Watanuki T; Ishimatsu N; Kawamura N; et al. Colossal Negative Thermal Expansion in $BiNiO_3$ Induced by Intermetallic Charge Transfer. Nat. Commun 2011, 2, 347. [PubMed: 21673668]

(7). Chen J; Nittala K; Forrester JS; Jones JL; Deng J; Yu R; Xing X The Role of Spontaneous Polarization in The Negative Thermal Expansion of Tetragonal $PbTiO_3$-Based Compounds. J. Am. Chem. Soc 2011, 133, 11114–11117. [PubMed: 21696173]

(8). Guillaume CÉ Recherches sur les aciers au nickel. Dilatations Aux Tempeŕatures eĺeveés; Reśistance eĺectrique. CR Acad. Sci 1897, 125, 18.

(9). Álvarez-Alonso P; Gorria P; Blanco JA; Sańchez-Marcos J; Cuello GJ; Puente-Orench I; Llamazares JLS; Rodriguez-Velamazan JA; Garbarino G; de Pedro I; et al. Magnetovolume and Magnetocaloric Effects in Er2Fe17. Phys. Rev. B: Condens. Matter Mater. Phys 2012, 86, 184411.

(10). Song YZ; Chen J; Liu X; Wang CC; Gao Q; Li Q; Hu L; Zhang J; Zhang S; Xing X Structure, Magnetism, and Tunable Negative Thermal Expansion in (Hf,Nb)Fe2 Alloys. Chem. Mater 2017, 29, 7078–7082.

(11). Zhao YY; Hu FX; Bao LF; Wang J; Wu H; Huang QZ; Wu R-R; Liu Y; Shen F-R; Kuang H; et al. Giant Negative Thermal Expansion in Bonded MnCoGe-Based Compounds with Ni_2In-Type Hexagonal Structure. J. Am. Chem. Soc 2015, 137, 1746–1749. [PubMed: 25629796]

(12). Huang R; Liu Y; Fan W; Tan J; Xiao F; Qian L; Li L Giant Negative Thermal Expansion in NaZn13-Type La(Fe, Si, Co)13 Compounds. J. Am. Chem. Soc 2013, 135, 11469–11472. [PubMed: 23885928]

(13). Song YZ; Chen J; Liu X; Wang C; Zhang J; Liu H; Xing XR; Zhu H; Hu L; Lin K; et al. Zero Thermal Expansion in Magnetic and Metallic Tb(Co,Fe)2 Intermetallic Compounds. J. Am. Chem. Soc 2018, 140, 602–605. [PubMed: 29292996]

(14). Takenaka K; Takagi H Giant Negative Thermal Expansion in Ge-Doped Anti-Perovskite Manganese Nitrides. Appl. Phys. Lett 2005, 87, 261902.

(15). Wang C; Chu L; Yao Q; Sun Y; Wu M; Ding L; Yan J; Na Y; Tang W; Li G; et al. Tuning the Range, Magnitude, and Sign of the Thermal Expansion in Intermetallic Mn3(Zn,M)xN (M = Ag, Ge). Phys. Rev. B: Condens. Matter Mater. Phys 2012, 85, 220103.

(16). Greve BK; Martin KL; Lee PL; Chupas PJ; Chapman KW; Wilkinson AP Pronounced Negative Thermal Expansion from a Simple Structure: Cubic ScF3. J. Am. Chem. Soc 2010, 132, 15496–15498. [PubMed: 20958035]

(17). Hu L; Chen J; Xu J; Wang N; Han F; Ren Y; Pan Z; Rong Y; Huang R; Deng J; et al. Atomic Linkage Flexibility Tuned Isotropic Negative, Zero, and Positive Thermal Expansion in MZrF6 (M= Ca, Mn, Fe, Co, Ni, and Zn). J. Am. Chem. Soc 2016, 138, 14530–14533. [PubMed: 27783492]

(18). Attfield JP Condensed-Matter Physics: A Fresh Twist on Shrinking Materials. Nature 2011, 480, 465–466.

(19). Goodwin AL; Calleja M; Conterio MJ; Dove MT; Evans JS; Keen DA; Peters L; Tucker MG Colossal Positive and Negative Thermal Expansion in the Framework Material Ag3[Co(CN)6]. Science 2008, 319, 794–797. [PubMed: 18258911]

(20). Goodwin AL; Kennedy BJ; Kepert CJ Thermal Expansion Matching via Framework Flexibility in Zinc Dicyanometallates. J. Am. Chem. Soc 2009, 131, 6334–6335. [PubMed: 19385622]

(21). Duyker SG; Peterson VK; Kearley GJ; Ramirez-Cuesta AJ; Kepert CJ Negative Thermal Expansion in LnCo(CN)6 (Ln= La, Pr, Sm, Ho, Lu, Y): Mechanisms and Compositional Trends. Angew. Chem 2013, 125, 5374–5378.

(22). Gao Q; Chen J; Sun Q; Chang D; Huang Q; Wu H; Sanson A; Milazzo R; Zhu H; Li Q; et al. Switching between Giant Positive and Negative Thermal Expansions of A YFe(CN)6-based Prussian Blue Analogue Induced by Guest Species. Angew. Chem., Int. Ed 2017, 56, 9023–9028.

(23). Zheng XG; Kubozono H; Yamada H; Kato K; Ishiwata Y; Xu CN Giant Negative Thermal Expansion in Magnetic Nanocrystals. Nat. Nanotechnol 2008, 3, 724–726. [PubMed: 19057591]

(24). van Schilfgaarde M; Abrikosov IA; Johansson B Origin of The Invar Effect in Iron-Nickel Alloys. Nature 1999, 400, 46–49.

(25). Rebello A; Neumeier JJ; Gao Z; Qi Y; Ma Y Giant Negative Thermal Expansion in La-Doped CaFe2As2. Phys. Rev. B: Condens. Matter Mater. Phys 2012, 86, 104303.

(26). Fujishita H; Hayashi Y; Saito M; Unno H; Kaneko H; Okamoto H; Ohashi M; Kobayashi Y; Sato M X-Ray Diffraction Study of Spontaneous Strain in Fe-Pnictide Superconductor, NdFeAsO0.89 F0.11. Eur. Phys. J. B 2012, 85, 52–57.

(27). Sleight A Materials Science: Zero-Expansion Plan. Nature 2003, 425, 674–676. [PubMed: 14562086]

(28). Nix FC; MacNair D The Thermal Expansion of Pure Metals: Copper, Gold, Aluminum, Nickel, and Iron. Phys. Rev 1941, 60, 597.

(29). Miracle DB Metal Matrix Composites–from Science to Technological Significance. Compos. Sci. Technol 2005, 65, 2526–2540.

(30). Della Gaspera E; Tucker R; Star K; Lan EH; Ju YS; Dunn B Copper-Based Conductive Composites with Tailored Thermal Expansion. ACS Appl. Mater. Interfaces 2013, 5, 10966–10974. [PubMed: 24175870]

(31). Ruch PW; Beffort O; Kleiner S; Weber L; Uggowitzer PJ Selective Interfacial Bonding in Al (Si)–Diamond Composites and Its Effect on Thermal Conductivity. Compos. Sci. Technol 2006, 66, 2677–2685.

(32). Ryelandt S; Mertens A; Delannay F Al/Stainless-Invar Composites with Tailored Anisotropy for Thermal Management in Light Weight Electronic Packaging. Mater. Des 2015, 85, 318–323.

(33). Vogelsang M; Arsenault RJ; Fisher RM An in Situ HVEM Study of Dislocation Generation at Al/SiC Interfaces in Metal Matrix Composites. Metall. Trans. A 1986, 17, 379–389.

(34). Mohn P A Century of Zero Expansion. Nature 1999, 400, 18–19.

(35). Moessner R; Ramirez AP Geometrical Frustratio. Phys. Today 2006, 59, 24.

(36). Tomiyoshi S; Yamaguchi Y; Nagamiya T Triangular Spin Configuration and Weak Ferromagnetism of Mn3Ge. J. Magn. Magn. Mater 1983, 31, 629–630.

(37). Cable JW; Wakabayashi N; Radhakrishna P Magnetic Excitations in the Triangular Antiferromagnets Mn3Sn and Mn3Ge. Phys. Rev. B: Condens. Matter Mater. Phys 1993, 48, 6159.

(38). Chen J; Gao Q; Sanson A; Jiang X; Huang Q; Carnera A; Lin K Tunable Thermal Expansion in Framework Materials through Redox Intercalation. Nature Commun 2017, 8, 14441. [PubMed: 28181576]

(39). Nakamura Y Magnetovolume Effects in Laves Phase Intermetallic Compounds. J. Magn. Magn. Mater 1983, 31, 829–834.

(40). Morellon L; Blasco J; Algarabel PA; Ibarra MR Nature of the First-Order Antiferromagnetic-Ferromagnetic Transition in the Ge-rich Magnetocaloric Compounds Gd5(SixGe1–x)4. Phys. Rev. B: Condens. Matter Mater. Phys 2000, 62, 1022.

(41). Roy SB; Perkins GK; Chattopadhyay MK; Nigam AK; Sokhey KJS; Chaddah P; Caplin AD; Cohen LF First Order Magnetic Transition in Doped $CeFe_2$ Alloys: Phase Coexistence and Metastability. Phys. Rev. Lett 2004, 92, 147203. [PubMed: 15089570]

(42). Sandratskii LM; Kübler, J. Role of Orbital Polarization in Weak Ferromagnetism. Phys. Rev. Lett 1996, 76, 4963. [PubMed: 10061424]

(43). Takenaka K; Ichigo M; Hamada T; Ozawa A; Shibayama T; Inagaki T; Asano K Magnetovolume Effects in Manganese Nitrides with Antiperovskite Structure. Sci. Technol. Adv. Mater 2014, 15, 015009.

(44). Song X; Sun Z; Huang Q; Rettenmayr M; Liu X; Seyring M; Li G; Rao G; Yin F Adjustable Zero Thermal Expansion in Antiperovskite Manganese Nitride. Adv. Mater 2011, 23, 4690–4694. [PubMed: 21913237]

(45). Deng S; Sun Y; Wu H; Huang Q; Yan J; Shi K; Malik MI; Lu H; Wang L; Huang R; et al. Invar-Like Behavior of Antiperovskite $Mn_{3+x}Ni_{1-x}N$ Compounds. Chem. Mater 2015, 27, 2495–2501.

(46). Ibarra MR; Algarabel PA; Marquina C; Blasco J; Garcia J Large Magnetovolume Effect in Yttrium Doped La-Ca-Mn-O Perovskite. Phys. Rev. Lett 1995, 75, 3541–3544. [PubMed: 10059612]

(47). Takenaka K; Takagi H Magnetovolume Effect and Negative Thermal Expansion in Mn3(Cu1−xGex)N. Mater. Trans 2006, 47, 471–474.

(48). Sayetat F; Fertey P; Kessler M An Easy Method for the Determination of Debye Temperature from Thermal Expansion Analyses. J. Appl. Crystallogr 1998, 31, 121–127.

(49). Moriya T; Usami K Magneto-volume Effect and Invar Phenomena in Ferromagnetic Metals. Solid State Commun 1980, 34, 95–99.

(50). Fujita A; Fukamichi K; Wang JT; Kawazoe Y Large Magnetovolume Effects and Band Structure of Itinerant-electron Metamagnetic La(FexSi1−x)13 Compounds. Phys. Rev. B: Condens. Matter Mater. Phys 2003, 68, 104431.

(51). Drak M; Dobrzański, L. A. Hard Magnetic Materials Nd-Fe-B/Fe with Epoxy Resin Matrix. J. Achiev. Mater. Manuf. Eng 2007, 24, 63–66.

(52). Zhang H; Sun Y; Niu E; Hu F; Sun J; Shen B Enhanced Mechanical Properties and Large Magnetocaloric Effects in Bonded La(Fe,Si)13-Based Magnetic Refrigeration Materials. Appl. Phys. Lett 2014, 104, 062407.

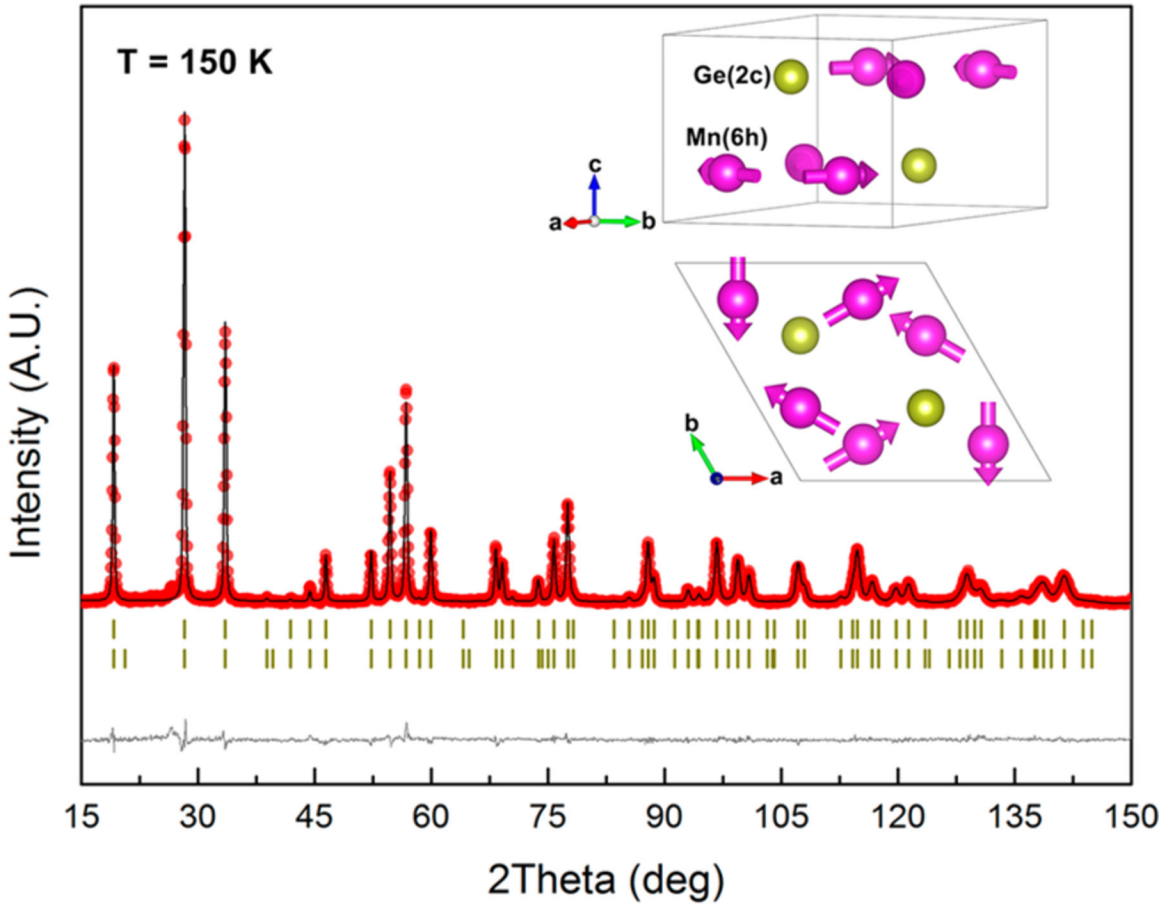

Figure 1.

Magnetic structure of NTE Mn_3Ge, determined via neutron powder diffraction. The space group is $P6_3/mmc$. The observed (red circles), calculated (black line), and differential (gray line at bottom of figure) patterns are shown for the full-profile refinement of Mn_3Ge at $T = 150$ K. The vertical ticks mark the calculated positions of nuclear and magnetic reflections. The inset shows the magnetic and crystal structures of Mn_3Ge.

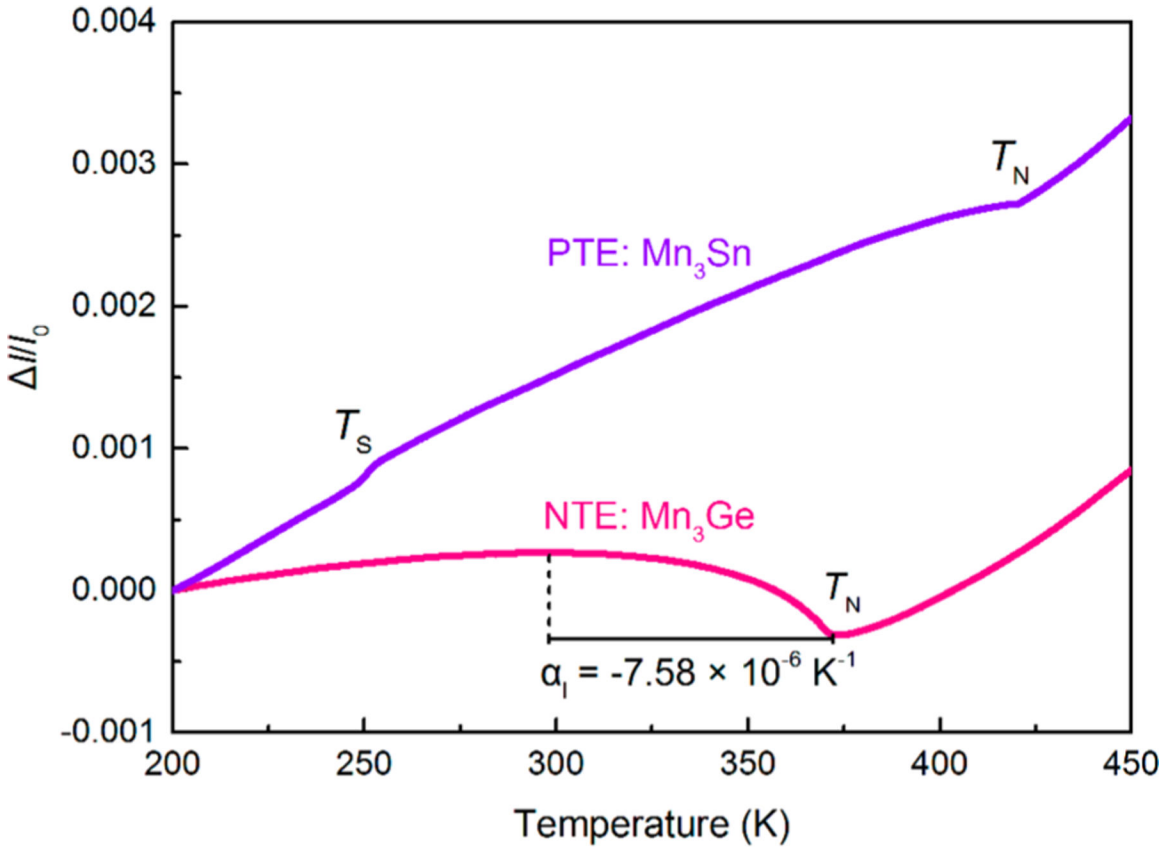

Figure 2.

Opposite thermal expansion in the isostructural antiferromagnetic intermetallics of Mn_3Ge and Mn_3Sn determined by a dilatometer ($\Delta l/l_0$). NTE is observed in Mn_3Ge, whereas PTE in the isostructural Mn_3Sn. T_s and T_N are the tempratures of magnetic transition.

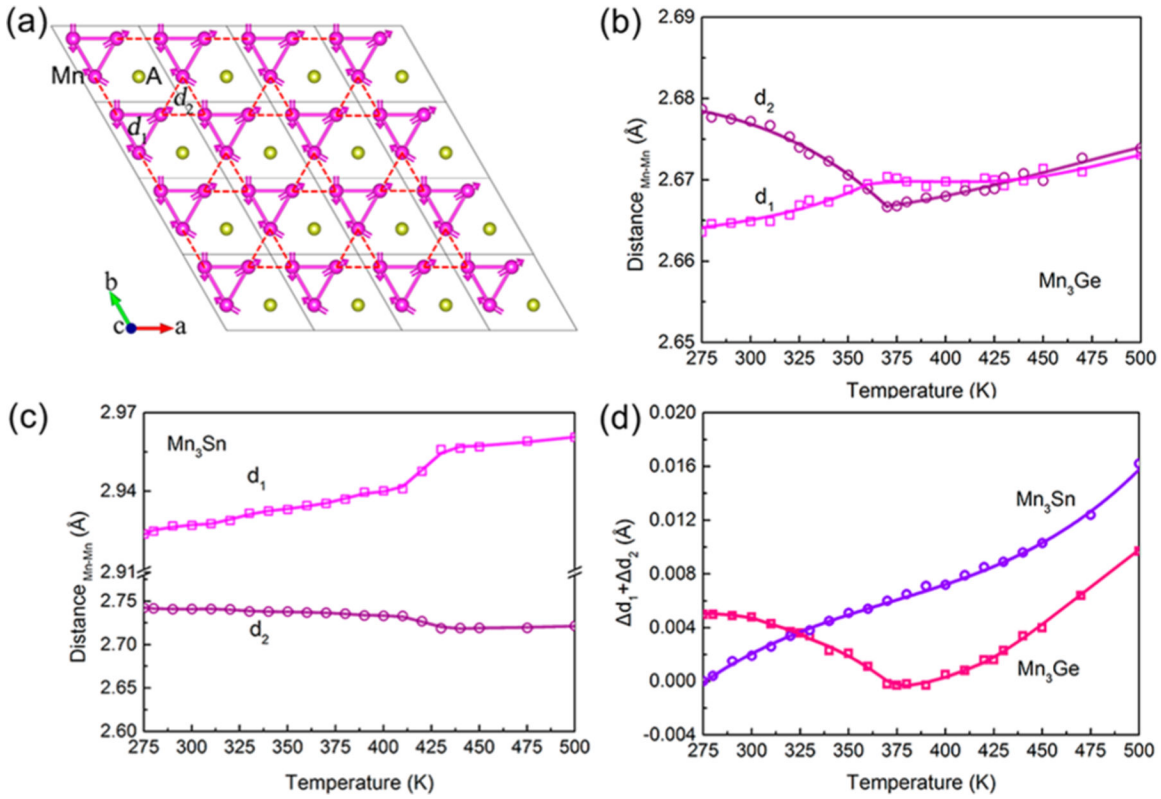

Figure 3.

Temperature dependence of bond distances between different sites of magnetic Mn atoms for NTE Mn_3Ge and PTE Mn_3Sn. (a) A layer of atoms in ab plane of $4 \times 4 \times 1$ supercell for Mn_3A (A = Ge and Sn), d_1 and d_2 mean the bond distances of Mn–Mn (I) and Mn–Mn (II) in the ab plane, respectively. Temperature dependence of d_1 and d_2 for (b) Mn_3Ge, and (c) Mn_3Sn. (d) Temperature dependence of relative change of $(\Delta d_1 + \Delta d_2)$ $\Delta d_1+\Delta d_2$ for Mn_3A (A = Ge and Sn).

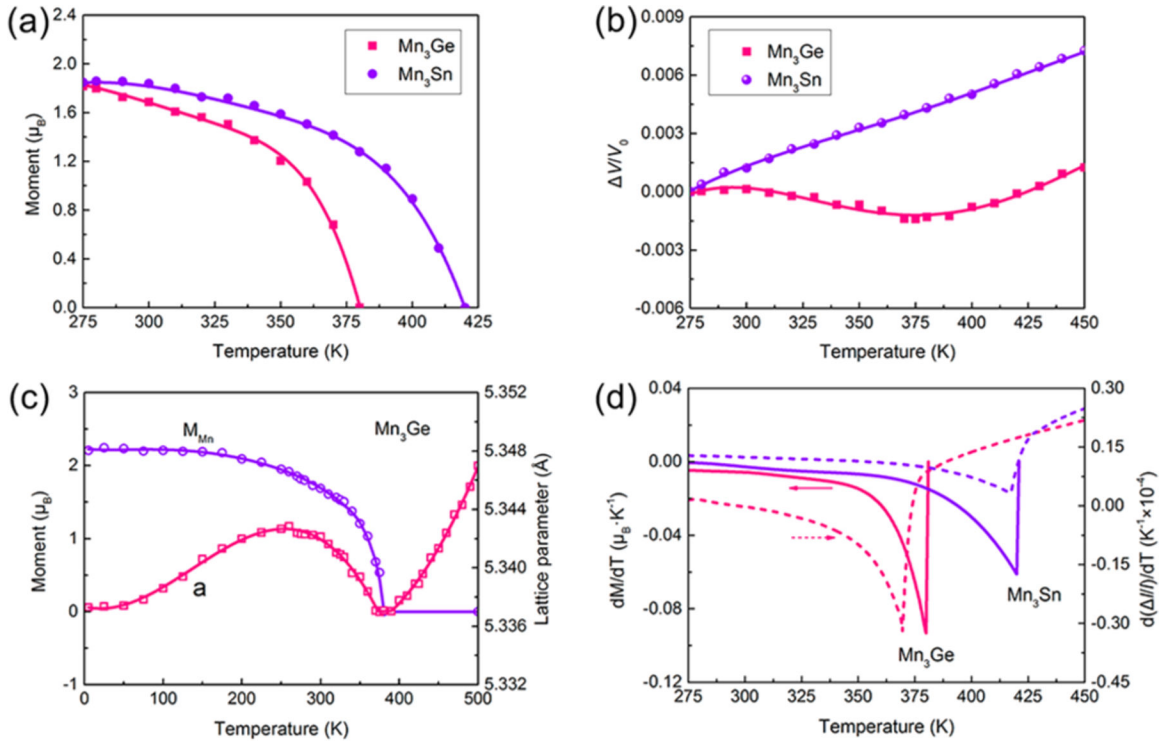

Figure 4.

NTE mechanism of Mn_3Ge. Temperature dependence of (a) the Mn moments of Mn_3Ge and Mn_3Sn, (b) the relative change in unit cell volume of Mn_3Ge and Mn_3Sn, (c) the Mn moment and lattice parameter a of Mn_3Ge, and (d) dM/dT and $d(\Delta l/l)/dT$ of Mn_3Ge and Mn_3Sn.

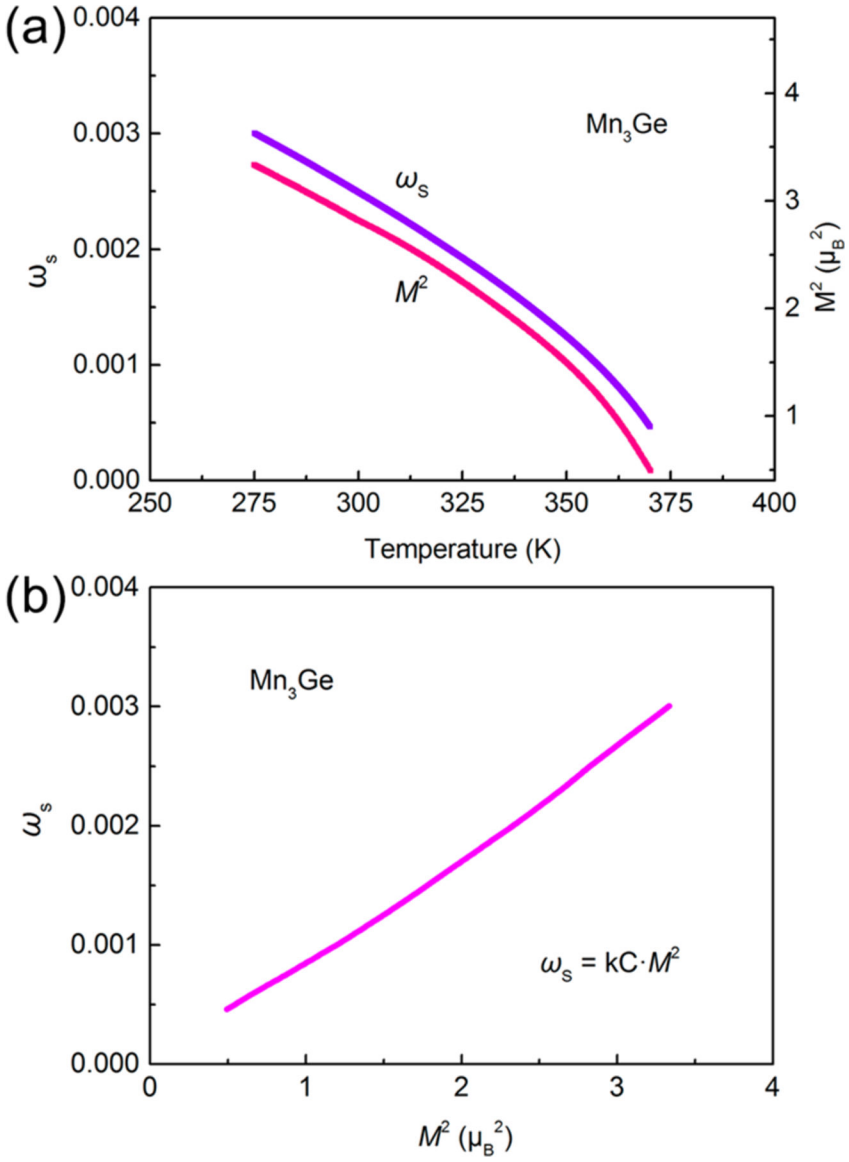

Figure 5.

(a) Temperature dependence of the square of Mn moment $\left(M^2\right)$ and spontaneous magnetostriction (ω_s) in Mn_3Ge. (b) Quantitative relationship between M^2 and ω_s.